FTIR Studies of O(^{3}P) Atom Reactions with CSe$_2$, SCSe, and OCSe

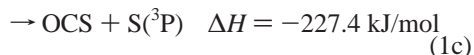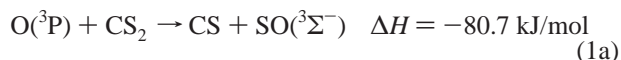**Shuping Li, Tsz Sian Chwee, and Wai Yip Fan***

Department of Chemistry, National University of Singapore, 3 Science Drive 3, Singapore 117543

Received: September 10, 2005; In Final Form: October 31, 2005

The overall rate coefficients of the reactions of CSe$_2$, SCSe, and OCSe with O(^{3}P) atom have been determined to be $k_{CSe_2} = (1.4 \pm 0.2) \times 10^{-10}$ cm^3 molecule^{-1} s^{-1}, $k_{SCSe} = (2.8 \pm 0.3) \times 10^{-11}$ cm^3 molecule^{-1} s^{-1}, and $k_{OCSe} = (2.4 \pm 0.3) \times 10^{-11}$ cm^3 molecule^{-1} s^{-1} at 301−303 K using Fourier transform infrared (FTIR) absorption spectroscopy. The measurements have been accomplished by calibrating against the literature value of the rate coefficient for O(^{3}P) with CS$_2$ (4×10^{-12} cm^3 molecule^{-1}s^{-1}). A product channel giving OCSe in $32.0 \pm 4.2\%$ yield has been found for the O + CSe$_2$ reaction. Although CO was also detected, its generation could be attributed to subsequent reactions of OCSe with O atoms. The corresponding reaction for O + SCSe gives OCS and OCSe as observable products, with their yields given as 32.2 ± 4.5 and $30.2 \pm 3.3\%$, respectively. Computational studies using UB3LYP/aug-cc-PVTZ methods have been used particularly to determine the reaction pathways for the channels in which OCS or OCSe is produced.

Introduction

The reaction of oxygen (^{3}P) atom with carbon disulfide, CS$_2$, has received considerable attention for its role in atmospheric chemistry, especially in the elucidation of global sulfur cycle leading to acid rain.[1] Three main product channels have been identified for this reaction:[2]

$$O(^3P) + CS_2 \rightarrow CS + SO(^3\Sigma^-) \quad \Delta H = -80.7 \text{ kJ/mol} \tag{1a}$$

$$\rightarrow CO + S_2(^3\Sigma^-_g) \quad \Delta H = -347.8 \text{ kJ/mol} \tag{1b}$$

$$\rightarrow OCS + S(^3P) \quad \Delta H = -227.4 \text{ kJ/mol} \tag{1c}$$

Cheng et al. has studied the dynamics of the dominant channel 1a by examining the vibrational state distributions of CS($^1\Sigma$) and SO($^3\Sigma$) using laser-induced fluorescence spectroscopy.[3] Cooper et al. used tunable infrared diode laser absorption spectroscopy (TDLAS) to determine a value of 2.8 for the branching ratio of (1c)/(1b).[2] Other related studies include a study of the oxidation of CS$_2$ at high temperatures, temperature-dependent kinetics for the determination of the activation energy of (1a), reactive scattering using crossed molecular beams, and chemiluminescence where the S$_2$ product of (1b) was identified.[4−7] In addition, the kinetics of the reaction of carbon monosulfide, CS, with O(^{3}P) atoms were also carried out.[8]

However we found that oxygen atom reactions with carbon chalcogenide species such as carbon diselenide, CSe$_2$, and carbon selenide sulfide, SCSe, have not been explored. Only one related investigation where the vibrational distribution of highly excited CO products after UV photolysis of a mixture containing nitrogen dioxide, NO$_2$, and CSe$_2$ was measured.[9] In this work, Fourier transform infrared (FTIR) absorption spectroscopy is used to extend the scope of O(^{3}P) atom reactions to CSe$_2$ and SCSe under static cell conditions. Although these Se-containing species are less abundant in the atmosphere, it is

still of interest to compare and contrast the effect of chalcogen substitution in CX$_1$X$_2$ (X = S, Se, or O) on their reactions with O(^{3}P) atoms. FTIR spectroscopy is ideal for broadband monitoring of the changes in the chalcogenide precursor and product concentrations upon O atom reactions. The generation of O(^{3}P) atoms is accomplished by using UV xenon lamp photolysis of NO$_2$.[2] Apart from examining the primary reactions, some secondary processes such as the reactions of O atoms with the product OCSe will be studied as well. Computational studies of the vibrational frequencies and band strengths of the species involved and the energies and geometries of reactive intermediates and transition states in these reactions will be determined. However, the assumed dominant channel of the O/CSe$_2$ system which produces CSe and SeO could not be directly investigated under static cell conditions. Its importance will be inferred by measuring and then subtracting out the contributions from other product channels. Such reactions would be best conducted using flow cell reactors, but the difficulty of obtaining large amount of CSe$_2$ and SCSe precludes their study here.

Experimental Section

CS$_2$ was purchased from Ajax Chemicals and distilled before use. Cylinders of NO, NO$_2$, OCS, and SF$_6$ gases were available from Linde gas and used without further purification. Because of the difficulty of obtaining commercial CSe$_2$ and SCSe samples, their syntheses have to be carried out. A literature search revealed that CSe$_2$ could be produced by passing dichloromethane vapor over hot selenium powder at 700 °C while SCSe was made by passing CS$_2$ over iron(II) selenide at 650 °C.[10,11] However attempts using these methods often resulted in severe contamination by CH$_2$Cl$_2$ or CS$_2$ despite careful steps taken for sample purification. Therefore an alternative method was devised in order to obtain gaseous samples of the chalcogenides from silver selenocyanate salts. AgNCSe was synthesized from an equimolar reaction of potassium selenocyanate, KNCSe (97%, Aldrich), with AgNO$_3$ aqueous solution. Typically, CSe$_2$ was generated from the vacuum decomposition (250−300 °C) of AgNCSe (1−2 g) in a 15 cm long, 3 cm diameter glass cell equipped with CaF$_2$

* Corresponding author. Fax: 65-67791691. E-mail: chmfanwy@nus.edu.sg.

windows for passage of the FTIR beam. Upon inspection by FTIR spectroscopy, the main decomposition product was CSe_2 ($\nu = 1300$ cm^{-1}) with a little amount of HCN ($\nu = 3314$ cm^{-1}, <1% CSe_2). The latter presumably arose due to reactions with hydrogen contaminants on the wall of the gas cell. Due to the differences in boiling points, HCN could be gradually removed after CSe_2 was collected in a dry ice/acetone trap. It was estimated that, during each synthesis, about 15−20 Torr of CSe_2 could be generated in a total volume of 500 cm^3; this amount was sufficient for a few kinetic runs in the static cell. For the production of SCSe, AgNCSe (0.5−3 g) and silver thiocyanate, AgNCS (0.5−3 g, Aldrich, 99%), were mixed and decomposed together at similar temperatures, yielding vapors containing the three expected products, CS_2 ($\nu = 1520$ cm^{-1}), SCSe ($\nu = 1435$ cm^{-1}), and CSe_2.[12] The production of exclusively SCSe was attempted by varying the ratio of the salt precursors, but it was unsuccessful because the resulting vapor contained either copious amounts of CS_2 at high ratios of AgNCS to AgNCSe or very little SCSe at low ratios of AgNCS to AgNCSe. However, contamination with CSe_2 could easily be removed by UV photodissociation at 254 nm.[13] Reddish solids attributed to selenium and carbon deposits were produced upon photolysis. Unfortunately, CS_2 could not be eliminated using the same method or by cold traps, so experiments carried out on SCSe always contained some amount of CS_2. Despite this, the simple method of decomposing the silver salts using their cyanate salts offered a very convenient way of generating CSe_2 or SCSe vapor.

A typical photolysis experiment would begin with the addition of carbon chalcogenide (3−10 Torr), NO_2 (3−20 Torr), and the buffer gas, SF_6 (≈1 bar), into the gas cell placed in the sample compartment of a Nicolet Nexus 870 FTIR spectrometer in a dark room. A capacitance gauge (MKS; range, 0.01−1000 Torr; accuracy ≈ 0.005 Torr) was used for gas pressure determination. O(^{3}P) atoms were generated by a broadband Xenon lamp (350−380 nm, 100 W) irradiation of NO_2. The lamp was fixed at 2 cm away from the main body of the glass cell. The temperature recorded by a thermocouple attached onto the outer wall of the cell showed an increase of 0.1−0.2 K during irradiation. However the laboratory temperature variation was larger (≈2 K), and hence the reaction temperature was quoted as occurring in the range of 301−303 K. A fiber optic cable placed at a fixed position of 1 cm away from the cell was used to direct a small portion of the radiation into an Acton Research monochromator (30 cm focal length) for monitoring the lamp output. The photolysis of the reaction mixture would only be initiated once a constant output of radiation from the lamp could be maintained, as monitored using the fiber optic cable. Unlike a laser, the broadband radiation is not expected to induce multiphoton and secondary processes which might affect the kinetic measurements. Nevertheless, the progress of the reactions under strong and weak irradiation could be easily compared by reducing the lamp power five times (≈20 W) but at the expense of a much longer irradiation time. We found that different irradiation power gave the same results for the kinetic runs; hence, multiphoton processes were kept to a minimum in our experiments. For experiments that required a mercury (Hg) lamp of 254 nm radiation, a quartz cell of similar size (15 cm long, 2.5 cm diameter) was used instead, while all other conditions were maintained as usual.

FTIR spectroscopy was used to record the decay and appearance of vibrational bands of reactants and products upon NO_2 photolysis. Table 1 lists the vibrational frequencies of the molecules monitored during the reaction. Typically, an IR

TABLE 1: Experimental and Calculated Vibrational Frequencies and Band Intensities (after Scaling) for the Various Molecules Investigated Here[a]

molecule	expt ν^b(cm^{-1})	calc ν(cm^{-1})	expt $I_{vib}{}^c$ (km/mol)	calc $I_{vib}{}^d$ (km/mol)
CO	2143	2207	62	80 (65)
CO_2	2349	2401	530	675 (547)
CS_2	1535	1550	597	684 (554)
CSe_2	1300	1322		546 (442)
SCSe	1435	1453		626 (507)
OCS	2062	2108	634	763 (618)
OCSe	2034	2075		769 (623)

[a] All the bands here have been used as spectroscopic probes for measurement of rates of reaction. The concentration limits of detection are also given here for each molecule using the respective vibrational band. [b] Except for CO, these values represent the asymmetric stretching vibrational frequencies. [c] Reference 14. [d] Scaled intensities in parentheses (factor = 0.81).

spectrum (range, 1000−3500 cm^{-1}; resolution, 1 cm^{-1}; average 16 scans) was collected every 1 min interval. The absorbances of the reactants were kept low (<20%) by adjusting their vapor pressures such that Beer−Lambert's law could be reliably used to form a linear relationship between absorbance and concentration. Purging of the spectrometer with N_2 was carried out to reduce interference from water and CO_2. This is especially important in experiments for which the appearance rate of CO_2 in the gas cell was to be measured accurately. Whenever possible, we used initial rate measurements to probe the kinetics during the early stages of irradiation. Typically this duration ranged from 0 to 5 min or slightly longer if the irradiation power was reduced. Initial rates measurements also served to minimize contributions from secondary reactions caused by product buildup. Each experiment was repeated 4−6 times, and uncertainty in the rate coefficient or branching ratio was quoted to 3σ deviation. The rate coefficients or product concentration ratios in their final form, i.e., after data analysis, are listed in Table 2 together with the previously determined rates from the O/CS_2 and O/OCS systems.

Results

A. Concentration Analysis. Since the measured infrared absorbance, Abs(ν) was related to concentration, c, via the Beer−Lambert law (Abs(ν) = $\epsilon(\nu)cl$ for small absorbances, l = 15 cm path length), the molar absorptivities, $\epsilon(\nu)$, of the molecular vibrational bands need to be known or estimated, especially for studying the main products of the reaction. Although the total vibrational band intensity, I_{vib}, values for each of the vibrations of CS_2, CO, and OCS have been determined,[14] a literature search reveals scarce data for the corresponding values for other species under investigation here, such as SCSe, OCSe, and CSe_2. The lack of data for these species may be due to the difficulty of obtaining pure samples; nevertheless, we have embarked on the calculation of I_{vib} of all relevant species using density functional method B3LYP and a fairly large basis set aug-cc-pvtz in Gaussian 98.[15] Molecular geometries were also optimized at this level of theory in order to obtain a good match between the experimental and calculated bond lengths and bond angles. Table 1 shows the calculated vibrational frequencies and band intensities as well as the previously determined experimental values, if any, for the molecules under study here. By comparing the experimental and computed intensities, excellent agreement could be found for CO, CO_2, CS_2, and OCS if an arbitrary scaling factor of 0.81 is applied to the calculated values, with a 4.6% discrepancy [=(1/N)($\Sigma(I_{calc} - I_{expt})/I_{calc}$); N = 4]. A scaling factor of <1 is

TABLE 2: Rate Coefficients and Branching Ratios Measured for the Reactions of O (^{3}P) Atoms with CS$_2$, CSe$_2$, SCSe, and OCSe

no.	reaction	rate coeff (cm^3 molecule^{-1} s^{-1})	percentage yield of products[a]
1	O(^{3}P) + CS$_2$ → products[b]	4.0×10^{-12}	[OCS]/[CO] = 2.8
2	O(^{3}P) + OCS → CO + SO[c]	$<1.0 \times 10^{-16}$	
3	O(^{3}P) + CSe$_2$ → products	$(1.4 \pm 0.2) \times 10^{-10}$	[OCSe] = 23.0 ± 4.0%
			[CO] = 9.0 ± 1.1%
4	O(^{3}P) + SCSe → products	$(2.8 \pm 0.3) \times 10^{-11}$	[OCS] = 32.2 ± 4.5%
			[OCSe] = 20.2 ± 3.0%
			[CO] = 10.0 ± 1.0%
5	O(^{3}P) + OCSe → CO + SeO	$(2.4 \pm 0.3) \times 10^{-11}$	[CO] ≈ 100%

[a] The ratios quoted here are the ones where the effects of secondary reactions have been taken into account. Thus they are not necessarily the raw experimental values. [b] Reference 2. [c] Reference 12.

typical of those used to scale vibrational frequencies as well. The good match gives some confidence in using the scaling factor for molecules for which the I_{vib} have not been determined yet. The band intensity is related to $\epsilon(\nu)$ by $I_{vib} = \int \epsilon(\nu) \, \delta\nu$, where $\delta\nu$ is the vibrational bandwidth. Since a typical bandwidth of the molecules here is 20–40 cm^{-1}, we have omitted the small line width contributions from the 1 cm^{-1} spectral resolution of the FTIR spectrometer. Thus the concentration can be estimated using the formula

$$c = (I_{vib}l)^{-1}\int \text{Abs}(\nu) \, \delta\nu$$

where the integral represents the area under the vibrational band.

For consistency purpose, we have used either the actual experimental value if possible or the scaled calculated values for all molecules in the determination of the rate constants in this work. As discussed later, the determination of many of the rate coefficients were carried out using pseudo-first-order approximations, which requires only a change in the concentration rather than the absolute value themselves. Hence the error incurred in the band intensity calculations is small except in cases where the product yields of molecules such as OCSe and CO are required. The minimum detectable concentration change of a molecular species could also be obtained by monitoring its absorbances as the reaction progressed and converting the values into concentrations using Beer–Lambert's law. Not surprisingly, molecules possessing intense vibrational bands such as OCS and OCSe have the lowest detection limit of concentration changes of ≈0.001 Torr or 3×10^{13} molecules cm^{-3}.

As mentioned, experimental errors were quoted to 3σ deviation. However for measurements that required the calculated intensity values such as product yields of OCSe, the error or discrepancy between the calculated and experimental values should be included. For example, the relationship between the errors is given by $(\Delta Z/Z)^2 = (\Delta A/A)^2 + (\Delta B/B)^2$, where ΔZ = overall error in the OCSe yield; Z = average yield; $\Delta A/A$ = experimental error in OCSe; and $\Delta B/B$ = 0.046, which is the error/discrepancy in calculated intensity. In all cases here, the experimental error was larger (>10%) than the error associated with the intensity calculations (4.6%).

B. Reactions of O (^{3}P) with CS$_2$ and OCS. The reaction of O(^{3}P) with CS$_2$ was first carried out to test whether our apparatus could be used to obtain reliable rate measurements. It is known that UV photolysis of NO$_2$ around 360–380 nm gives a unit quantum yield of O(^{3}P) atoms.[2] Using flash kinetic infrared spectroscopy, Cooper et al. found the [OCS]/[CO] ratio produced in this reaction to be 2.7.[2] We have used FTIR spectroscopy to measure the relative rate of appearance of these species by monitoring the evolution of CO (ν_{co} = 2143 cm^{-1}) and OCS (ν_{ocs} = 2062 cm^{-1}) absorptions. Our initial rate measurements gave an average [OCS]/[CO] ratio of 2.8 ± 0.2 over a range of

NO$_2$ and CS$_2$ pressures (5–10 Torr each); this is in good agreement with the above literature value.

In addition, we have also investigated the reaction of O with OCS to determine if CO might have been produced from this reaction. The small value of its rate coefficient ($<1 \times 10^{-16}$ cm^3 molecule^{-1} s^{-1})[12] implies that CO is not expected to be observed over a short irradiation time. A large pressure of OCS was therefore used with the possibility of generating more CO molecules for detection. However, the CO transitions were still unobservable despite a few hours of photolysis of 5 Torr NO$_2$ and 30 Torr of OCS. From these findings, we found that the data collected were consistent with previous studies of these reactions, thus lending support to the reliability of our system for extending the scope of similar reactions.

C. Reactions of O (^{3}P) atoms with CX$_1$X$_2$ (X$_1$ = Se; X$_2$ = O, S, or Se). Upon thermal decomposition of AgNCSe and/or AgNCS, all three carbon chalcogenides could be produced. The production of CS$_2$ was the most facile, and hence its IR signal was generally observed to be the strongest of the three species, while SCSe and CSe$_2$ tend to have similar intensities. Depending on the amount of silver salts used, it was possible to saturate the IR signals of all three chalcogenides. The absorbances of all three infrared bands remained unchanged even after 2–3 days, indicating their stability toward self-decompositions and wall decompositions.

Having produced a sufficient amount of CSe$_2$, the reaction of O(^{3}P) atoms with CSe$_2$ can be subsequently studied in the static cell. A few control experiments were carried out initially to investigate the effect of interference from unwanted reactions. First, the xenon lamp radiation was directed into a sample containing only CSe$_2$ but no photodissociation resulted from the process. Second, when NO$_2$ was added to CSe$_2$ (5 Torr) in the cell in the absence of photolysis, the IR spectra of CO and OCSe could not be detected, implying that the reaction of NO$_2$ with CSe$_2$ was very slow under our experimental conditions. Since NO is the product of NO$_2$ photolysis, the effect of mixing an excess of NO (10 Torr) with CSe$_2$ (5 Torr)) was also examined, but no reaction was observed. It was only upon xenon lamp photolysis in the presence of both NO$_2$ and CSe$_2$ that IR signals of CO and OCSe began to appear and increased in intensity with respect to the irradiation time. This observation indicated that it was indeed the O atoms produced from NO$_2$ photolysis that were responsible for generating CO and OCSe. Figure 1 shows a typical IR spectrum taken of the reaction mixture before and after photolysis, showing the decay of CSe$_2$ and appearance of CO and OCSe upon O(^{3}P) atom reactions. Since a minor production of OCSe from the thermal decomposition of AgNCSe was unavoidable, it could be easily subtracted from the much larger OCSe signals that came from the
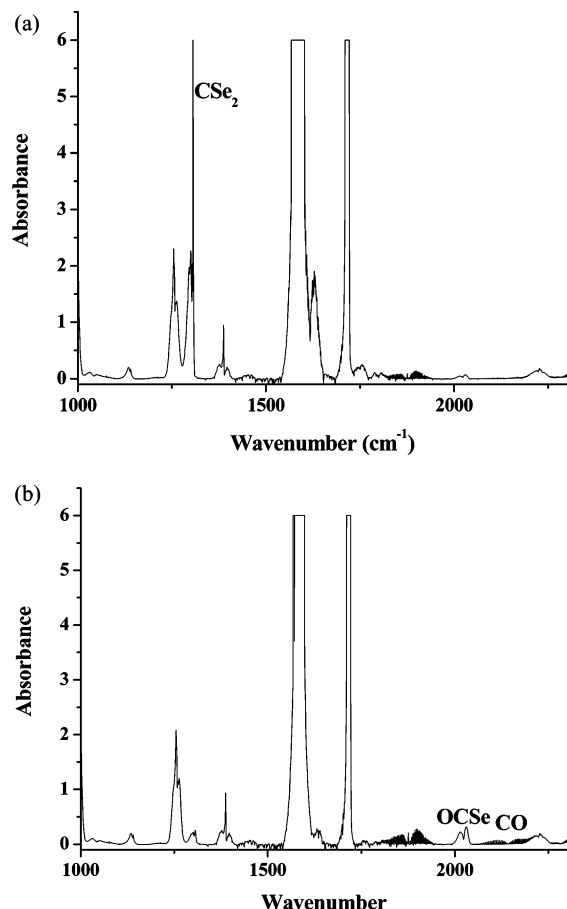
Figure 1. FTIR spectrum of CSe_2(10 Torr) + NO_2(20 Torr) in SF_6 buffer gas ($\approx$1 bar) before photolysis (a) and after photolysis (b). The CSe_2 infrared signal showed depletion, while the appearance of small signals of OCSe and CO could be observed. The intense bands around $1600-1750$ cm^{-1} belong to NO_2.

photolytic reaction. The product yields of OCSe and CO were measured over a range of NO_2 and CSe_2 pressures by comparing their appearance rates to the decay rate of CSe_2,

$$R_{CO} = k_{CO}/k_{CSe_2} = \Delta[CO]_t/\Delta[CSe_2]_t$$

$$R_{OCSe} = k_{OCSe}/k_{CSe_2} = \Delta[OCSe]_t/\Delta[CSe_2]_t$$

where $\Delta[X]_t$ represents the change in concentration of X at time, t; k_X is the appearance or decay rate of X. The linear plots of CO and OCSe production versus CSe_2 loss are shown in Figure 2. It was found that after repeating the experiments four to six times, the average yields of [OCSe] and [CO] were determined to be 23.0 ± 4.0 and $9.0 \pm 1.1\%$ during the initial stages of irradiation.

The overall reaction rate constants of CSe_2 with O atom could also be measured relative to the reaction between CS_2 and O atom. This was accomplished by deliberately adding CS_2 into the cell containing NO_2 and CSe_2 and allowing both CSe_2 and CS_2 to react competitively with O atoms. Since the rate coefficient of the latter reaction is known previously, the rate coefficient of the former reaction could then be determined. The relative rate k_{CSe_2}/k_{CS_2} was obtained by observing the disappearance of CSe_2 and CS_2 during the initial stages of irradiation.
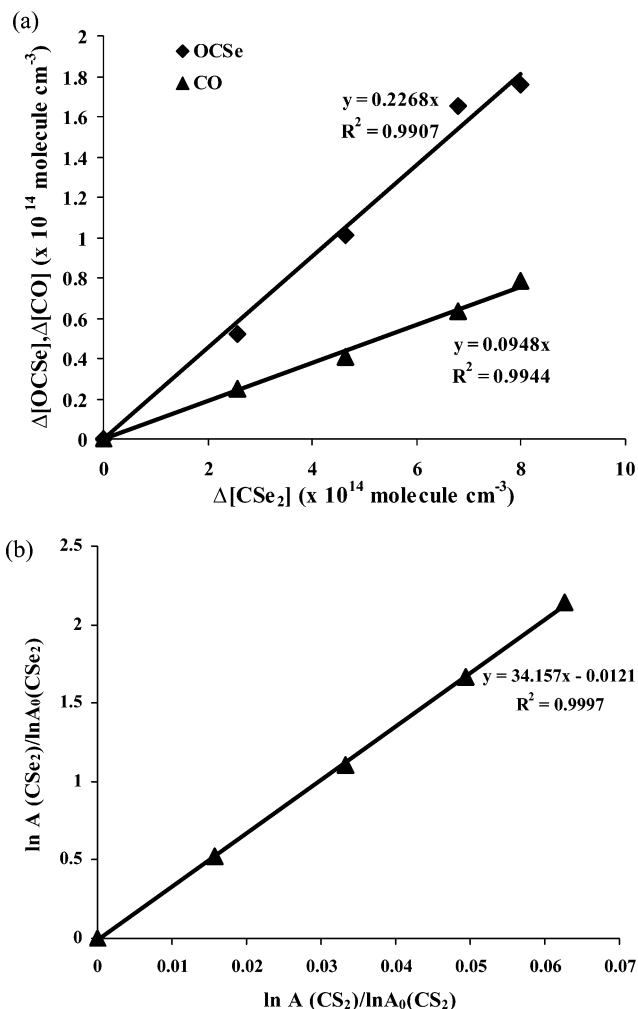

Figure 2. (a) Plot of OCSe and CO productions vs CSe_2 loss during early stages (5 min) of UV lamp photolysis of O/CSe_2; (b) plot of ln A_{CSe_2}/ln A_{0,CSe_2} versus ln A_{CS_2}/ln A_{0,CS_2} during UV lamp photolysis of O/CSe_2. A linear relationship was observed until all the CSe_2 has been completely reacted.

Since the amount of O atoms produced was far less than CS_2 or CSe_2, the reaction proceeds via pseudo-first-order kinetics:

$$\frac{\ln([CSe_2]_0/[CSe_2])}{\ln([CS_2]_0/[CS_2])} = k_{CSe_2}/k_{CS_2}$$

$$\frac{\ln[(A_{0,CSe_2}/\epsilon_{CSe_2}l)/(A_{CSe_2}/\epsilon_{CSe_2}l)]}{\ln[(A_{0,CS_2}/\epsilon_{CS_2}l)/(A_{CS_2}/\epsilon_{CS_2}l)]} = k_{CSe_2}/k_{CS_2}$$

$$\frac{\ln(A_{0,CSe_2}/A_{CSe_2}l)}{\ln(A_{0,CS_2}/A_{CS_2})} = k_{CSe_2}/k_{CS_2}$$

where the subscript 0 denotes the concentration [X] or absorbance A of species X at time zero (before photolysis). A linear relationship was indeed observed between $\ln(A_{0,CSe_2}/A_{CSe_2})$ and $\ln(A_{0,CS_2}/A_{CS_2})$ and the ratio k_{CSe2}/k_{CS_2} was estimated from the initial linear slope of the plots shown in Figure 2b. A value for the overall reaction rate of O with CSe_2, was then determined to be $k_{CSe_2} = (1.4 \pm 0.2) \times 10^{-10}$ cm^3 molecule^{-1} s^{-1} after substituting the value for $k_{CS_2} = 4.0 \times 10^{-12}$ cm^3 molecule^{-1} s^{-1}.[6] When the rates of change of the three species (CSe_2, OCSe, and CO) were compared, a ratio of $(100 \pm 2):(23.0 \pm 4.0):(9.0$

(a)

(b)

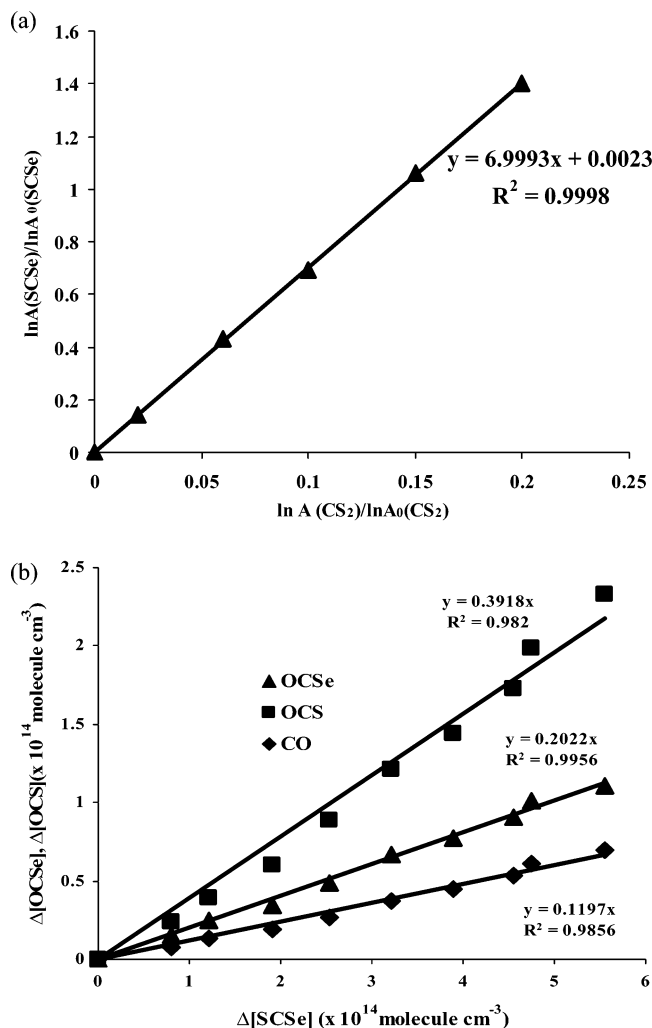
Figure 3. (a) Plot of ln A_{SCSe}/ln $A_{0,SCSe}$ versus ln A_{CS_2}/ln A_{0,CS_2} during UV lamp photolysis of O/SCSe. A linear relationship was observed until all the SCSe has been completely reacted. (b) Plots of OCSe, OCS, and CO formation vs SCSe decay for the reaction of O + SCSe in the presence of CS$_2$ during photolysis.

± 1.1) was obtained for CSe$_2$:OCSe:CO, respectively (with the negative sign indicating a signal decay).

The control experiments described earlier for the O/CSe$_2$ system were also performed for the O/SCSe/CS$_2$ system. Similar results were obtained, whereby it was only upon photolysis of NO$_2$ in a mixture of CS$_2$ and SCSe that CO, OCS, and OCSe first appeared. Although the production of SCSe was always accompanied by the presence of CS$_2$, this is advantageous because the competitive reaction of O(^{3}P) with CS$_2$ may again be used as the internal standard for determining the overall rate coefficient of O(^{3}P) with SCSe.

The decays of equal pressures of SCSe and CS$_2$ (5 Torr) signals were compared, and it was found that SCSe reacted 7 times faster with O atoms, hence with an overall rate constant of $k_{SCSe} = (2.8 \pm 0.3) \times 10^{-11}$ cm^3 molecule^{-1} s^{-1} (Figure 3a). The unsymmetrical SCSe molecule may react with O(^{3}P) to form either OCS or OCSe. The rates for the production of OCS, OCSe, and CO were measured to be about 3, 5, and 10 times slower, respectively, if compared against the decay rate of SCSe during the initial stages of irradiation (Figure 3b). In other words, the [SCSe]:[OCS]:[OCSe]:[CO] ratio could also be expressed as (100 ± 2.2):(34.5 ± 5.0):(20.2 ± 3.0):(10 ± 1.0). However, OCS could also be generated from the reaction of O with CS$_2$ albeit with a different rate. Since it has been

determined that CS$_2$ decays 7 times slower than SCSe and if the branching ratio for the production of OCS from CS$_2$ or SCSe is similar, then the OCS contributions from the O/CS$_2$ system are ≈14% of the total amount. However, it was possible in our experiments to synthesize about 50% more SCSe than CS$_2$; this reaction mixture was usually used for a better differentiation of the OCS branching ratio. We further estimate the contributions to OCS by CS$_2$ or SCSe by increasing the ratio of CS$_2$ to a fixed amount of SCSe in the reaction mixture and remeasuring the OCSe/OCS ratio again. If the O/CS$_2$ reaction contributes significantly, the signals of OCS will also increase correspondingly compared to OCSe, which comes only from SCSe. From the results of varying the reactant ratios ranging from [SCSe]/[CS$_2$] = 1.5:1 to 1:4, we could revise the overall [SCSe]:[OCS]:[OCSe]:[CO] ratio to be (100 ± 2.2):(32.2 ± 4.5):(20.2 ± 3.0):(10 ± 1.0).

The importance of secondary reactions involving OCSe was also considered since they could contribute to the generation of CO and perhaps CO$_2$ upon subsequent reactions with O atoms. The preparation of OCSe free from CSe$_2$ or SCSe contamination could be carried out in this manner. Starting from a reaction mixture containing CSe$_2$ and excess NO$_2$, 254 nm UV irradiation of the sample over time would result in OCSe being formed and CSe$_2$ being completed reacted. The major components of the gas mixture at the end of the 254 nm irradiation would be NO$_2$, NO, CO, and OCSe. Further photolysis of NO$_2$ would then allow the reaction of O with OCSe to proceed and its products to be monitored. A known pressure of CS$_2$ could also be added into the reaction mixture in a separate experiment run so that the rate coefficient of the reaction could be calibrated against k_{CS_2}. It was found that the OCSe IR signal decreased further upon reactions with O atoms but at a rate of about 5.8 times slower compared to O and CSe$_2$ reactions. This resulted in a rate coefficient for the O and OCSe reactions to be $k_{OCSe} = (2.4 \pm 0.3) \times 10^{-11}$ cm^3 molecule^{-1} s^{-1} (Figure 4a). In addition, only the increase of CO infrared signals (subtracted from CO already present in the mixture) was registered without any detectable formation of CO$_2$. Interestingly the magnitude of the decay rate of OCSe appeared to be very close to the appearance rate of CO, judging from a near-unity value (0.94) for the gradient of Figure 4b.

Discussion

The reaction rate coefficients k_{CSe_2} ((1.4 ± 0.2) × 10^{-10} cm^3 molecule^{-1} s^{-1}) and k_{SCSe} ((2.8 ± 0.3) × 10^{-11} cm^3 molecule^{-1} s^{-1}) have been measured to be 34 and 7 times larger than that of k_{CS_2} (4.0 × 10^{-12} cm^3 molecule^{-1} s^{-1}); this may be a result of lower activation barriers for these reactions. Qualitatively, it is not surprising to observe an increase in rates since the C=Se bond of CSe$_2$ or SCSe is weaker than the C=S bond of CS$_2$ and hence yielding relatively lower energy transition states as well. Because of the weaker C=Se bond, the O and OCSe (k_{OCSe} = (2.4 ± 0.3) × 10^{-11} cm^3 molecule^{-1} s^{-1}) reaction is also observed to proceed much faster than the corresponding O and OCS reaction ($k < 1.0 \times 10^{-16}$ cm^3 molecule^{-1} s^{-1}). Evidence gathered by the excellent match between the decay rate of OCSe with the appearance rate of CO upon O atom reactions suggests that only a single channel is open and the measured rate coefficient may be used to describe the single reaction, O + OCSe → CO + SeO.

Two products from the O/CSe$_2$ system were detected, i.e., OCSe and CO with the former being more abundant with product yields of 23.0 ± 4.0% compared to 9.0 ± 1.1%. The combined appearance rates of OCSe and CO are thus only a

(a)

(b)
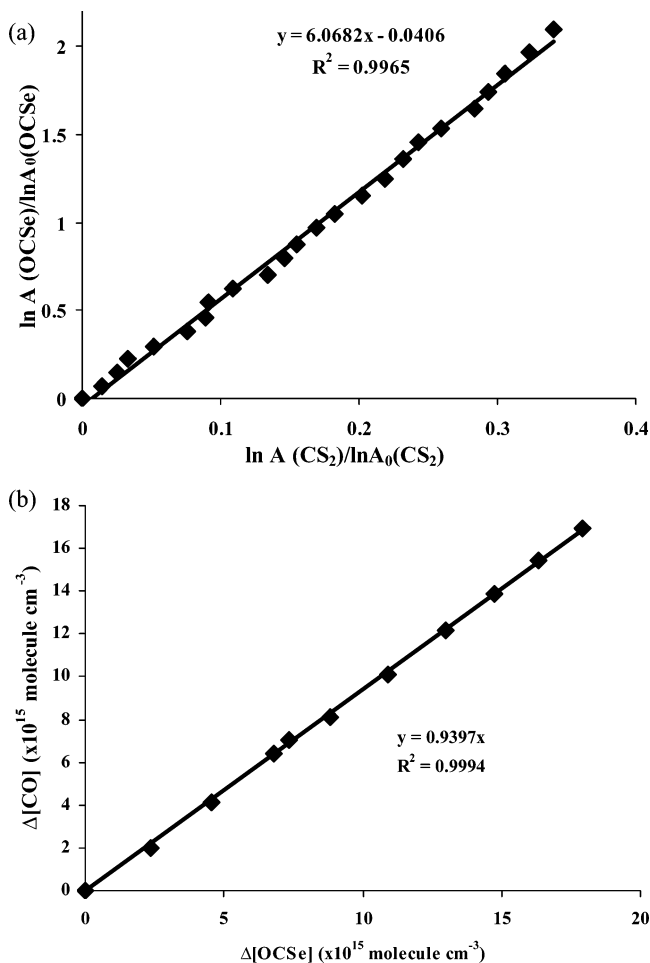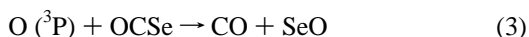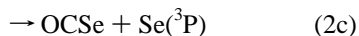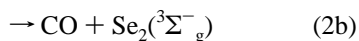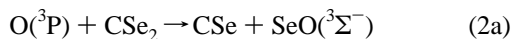

Figure 4. (a) Plot showing the decay of OCSe against the decay of CS$_2$ signals upon O atom reactions. (b) Plot of CO production vs OCSe loss during UV lamp photolysis (360−380 nm) of an O/OCSe mixture. No CO$_2$ was observed during the reaction.

fraction, about 32%, of the CSe$_2$ decay rate. This certainly implies that at least another product channel is open for the O/CSe$_2$ system. By analogy to reaction 1a of the O/CS$_2$ system, the channel could be attributed to O (^{3}P) + CSe$_2$ → CSe + SeO. The large discrepancy in the above measured rates would suggest that the production of CSe and SeO is the main reaction channel. The ratio of products generated by the O/CSe$_2$ system could then be expressed as CSe:OCSe:CO = (68 ± 5):(23.0 ± 4.0):(9.0 ± 1.1).

It is tempting at this stage to ascribe three reaction channels (represented by CSe, OCSe, and CO products) for the O/CSe$_2$ system, similar to those observed for the O/CS$_2$ system. However OCSe continues to react further with O atoms to yield exclusively CO with a rather large rate coefficient. This is certainly unlike the O/CS$_2$ system, where the slow reaction between O and OCS does not contribute significantly to the production of CO. For clarity sake, the possible reactions in the O/CSe$_2$ system may be written as

$$O(^3P) + CSe_2 \rightarrow CSe + SeO(^3\Sigma^-) \qquad (2a)$$

$$\rightarrow CO + Se_2(^3\Sigma_g^-) \qquad (2b)$$

$$\rightarrow OCSe + Se(^3P) \qquad (2c)$$

$$O(^3P) + OCSe \rightarrow CO + SeO \qquad (3)$$

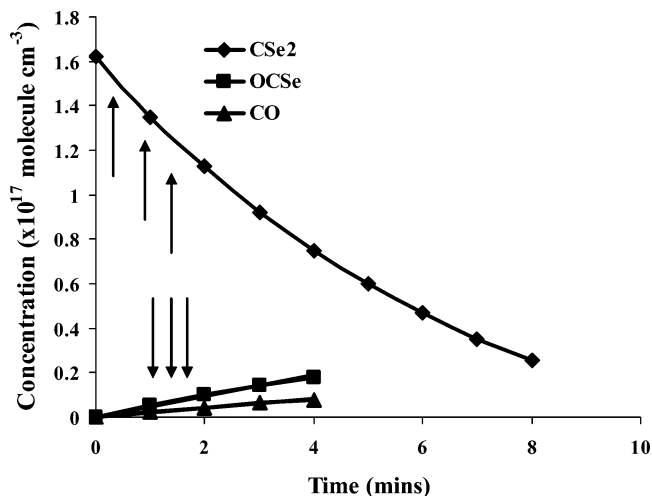The CO production could come from reactions 2b and 3. To

Figure 5. Plots of CSe$_2$, OCSe, and CO concentrations as a function of photolysis time in a reaction mixture containing 5 Torr CSe$_2$, 10 Torr NO$_2$. Arrows pointing upward indicate the tangents drawn for the estimation of O atom concentration. Arrows pointing downward indicate the sampling of three different times for the estimation of the contribution of O/OCSe reaction to CO production.

determine the relative importance of these two channels, the O atom concentrations need to be estimated first. This can be accomplished by examining the rate of decay of CSe$_2$ during the early stages of irradiation (see Figure 5), where
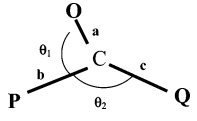
$$d[CSe_2]/dt = -k_{CSe_2}[O][CSe_2]$$

The concentration change of CSe$_2$ could be estimated by drawing a tangent to its decay curve at certain time intervals, and since both k_{CSe_2} and [CSe$_2$] are known, the O atom concentration could then be determined. Calculations carried out at three different early times as indicated in Figure 5 gave an average value of [O] = (5.0 ± 0.5) × 10^7 cm^{-3}. As expected, the concentration is rather low because of the low power irradiation used for the experiments. The CO contribution from the O/OCSe reaction could be approximated now that the O atom concentration is known. We first assume that all CO came from this reaction, thereby ignoring reaction 2b;

$$d[CO]/dt = k_3[O][OCSe]$$

Since k_3 has been measured and both [OCSe] and d[CO]/dt can be evaluated directly from Figure 5, the values for the left-hand and right-hand sides of the equation can be compared at different times of the reaction. When comparisons were made for three different times as indicated in the graph, it turns out that the left- and right-hand-side values were equal and thus the reaction of O with OCSe could perhaps fully account for the production of CO! If this were the case, reaction 2b is at most a minor channel on the basis of this analysis. Since some OCSe have reacted further to generate all the CO detected in the system, the branching ratio of reaction 2c would have been underestimated, and hence, it should be revised accordingly to include the CO contributions to 23% + 9% = 32%.

Similar analysis could also be carried out on the O/SCSe system. The product ratio of [OCS]:[OCSe]:[CO] has been found to be (32.2 ± 4.5):(20.2 ± 3.0):(10 ± 1.0). The probability of direct CO production from O and SCSe reaction is again in doubt. As usual, the [O] concentration could be determined to be 4.5 × 10^7 cm^{-3} from the early stage of irradiation for a NO$_2$-(15 Torr)/SCSe(7 Torr)/CS$_2$(9 Torr) mixture. Indeed, for the given concentration of [O], it appears that the O + OCSe

O(^{3}P) Atom Reactions with CSe$_2$, SCSe, and OCSe

J. Phys. Chem. A, Vol. 109, No. 51, 2005 **11821**

TABLE 3: Optimized Structures and Vibrational Frequencies of the Intermediates and Transition States in the O/CS$_2$, O/SCSe, and O/CSe$_2$ Systems Determined at the UB3LYP/aug-cc-PVTZ Level of Theory[a]

| structure	P, Q	a, b, c (Å)	θ_1 (deg), θ_2 (deg)	vibrational freq (cm^{-1})
A	S, S	1.95, 1.61,1.56	79, 162	431i, 247, 328, 402, 635, 1429
B	S, S	1.19, 1.78, 1.78	133, 94	289, 381, 508, 547, 606, 1798
C	S, S	1.16, 2.28, 1.64	119, 87	307i, 222, 394, 503, 750, 1992
D	Se, Se	2.07, 1.69, 1.75	76, 165	354i, 193, 242, 326, 378, 1240
E	Se, Se	1.18, 1.94,1.94	133, 94	178, 279, 450, 459, 495, 1812
F	Se, Se	1.16, 2.49, 1.79	118, 87	228i, 137, 321, 450, 561, 1993
G	S, Se	1.98, 1.56, 1.72	97, 170	473i, 177, 262, 334, 493, 1349
H	S, Se	1.18,1.72, 2.03	139, 93	209, 261, 457, 489, 666, 1830
I	S, Se	1.17, 2.30, 1.65	121, 90	211i, 205, 374, 492, 727, 1945
J	Se, S	1.15, 2.43, 1.78	117, 84	265i, 164, 348, 457, 576, 2020
K	Se, O	2.03, 1.75, 1.16	57, 179	395i, 361, 469, 637, 690, 2106

^{a} The imaginary frequencies of the transition states are denoted by i.
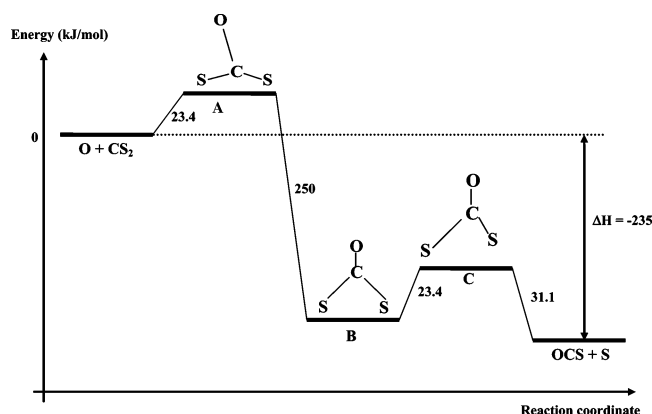
Figure 6. Energy level diagram for the O(^{3}P) + CS$_2$ → OCS + S(^{3}P) potential energy surface showing the intermediate and transition states computed at the UB3LYP/aug-cc-PVTZ level of theory.

secondary reactions could account for the entire CO produced during the initial stages of photolysis. Thus, the ratio of [OCS]: [OCSe]:[CO] is revised to 1.6:1.5:≈0. However the total appearance rate of these species could only account for 62% of the decay rate of SCSe. Similar to the O/CS$_2$ system, two other product channels could be assigned to the production of SeO and CS, and SO and CSe. Unfortunately the relative importance of the two channels could not be separately determined here; hence only one branching ratio of 38 ± 5% will be used to describe the contribution of these channels.

D. Computational Studies. Ab initio computational studies have been performed using Gaussian 98 to further understand and substantiate the experimental findings. Since OCSe has been detected as the main observable product in this work, we place emphasis on the computation of the (1c), (2c), and related reaction pathways for the O/SCSe system. The density functional theory (DFT) method of UB3LYP with aug-cc-PVTZ basis sets has been used for the optimization of the structures and energies of reactive intermediates and transition states in all the reactions of O(^{3}P) with CS$_2$, CSe$_2$, and SCSe (Table 3).[16]

Comparisons with the experimental values of the enthalpies of formation of the three channels of the O/CS$_2$ system were first made to check the reliability of the calculations. As shown in Figure 6, the reaction pathway leading to OCS and S (channel 1c) has been calculated for the O/CS$_2$ system on a triplet
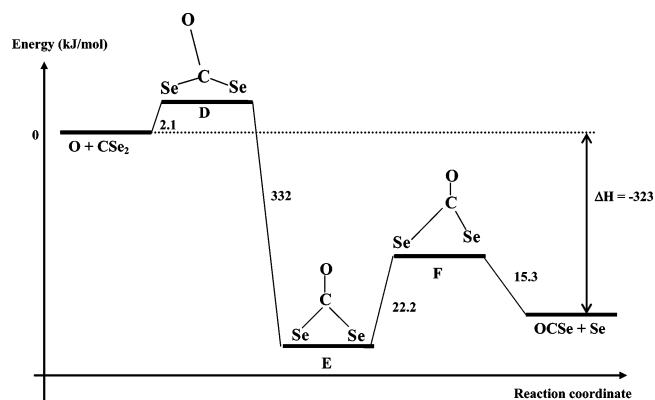
Figure 7. Energy level diagram for the O(^{3}P) + CSe$_2$ → OCSe + Se(^{3}P) potential energy surface showing the intermediate and transition states computed at the UB3LYP/aug-cc-PVTZ level of theory.

potential energy surface. The calculated enthalpy of formation, ΔH_r, of the overall reaction is −235 kJ/mol, which puts it in very good agreement with previously determined experimental values.[2] Several intermediates or transition states were found along this pathway as well. The first optimized transition state A depicts the oxygen atom approaching CS$_2$ at an ∠OCS angle of about 79°. Despite several attempts, we have been unable to find an optimized structure in which the O atom is directed perpendicularly (∠OCS = 90°) toward the C atom. Incidentally, a bent transition state rather than a collinear one was also found previously for the primary channel 1a.[3] An earlier study showed that the average kinetic energy of the O(^{3}P) atom following 355 nm photolysis corresponding to NO(X^{2}Π,v=0) state was 1833 cm^{-1}.[15] As the calculated activation energy turns out to be about 23 kJ/mol (1922 cm^{-1}), it is just low enough for the reaction to take place at rates measurable over a short time under our experimental conditions. Not surprisingly, this value is higher than the activation energy of the primary channel 1a, which was estimated to be about 420 cm^{-1}.[16] The transition-state structure also shows that the two sulfur atoms of the CS$_2$ moiety have bent away from the incoming O atom and will eventually lead to the intermediate COS$_2$ denoted as B. This intermediate B, which sits in a relatively deep potential energy well (250 kJ/mol) with respect to structure A, is also believed to be the precursor to channel 2b, where CO and S$_2$ are produced.[2] The C=O bond distance of 1.19 Å for B is only slightly longer than a typical carbonyl bond of organic molecules (1.15−1.17 Å). Further along the pathway, a second transition state C was found in which one of the C=S bonds lengthens as the sulfur atom of that bond begins to pull away, leaving behind an OCS moiety which has a quasilinear structure with an obtuse angle of 154°. The dissociative C−S bond distance at 2.28 Å is considered rather long but consistent with C being a late transition state and hence productlike in structure.

As expected, similar transition states and intermediates of the reaction pathway were also computed for the O/CSe$_2$ system with ΔH_r = −323 kJ/mol (Figure 7). The first activation energy leading to structure D for this system is only 2.1 kJ/mol. This almost barrierless reaction explains the experimental data in which the production of OCSe from CSe2 is >37 times faster than the production of OCS from CS$_2$. The transition states, D and F, also closely resemble their sulfur counterparts in structure. The intermediate COSe$_2$ denoted by E occupies a deep potential well relative to D and forms the lowest energy state of the reaction pathway for the O/CSe$_2$ system.

For the O/SCSe system shown in Figure 8, the enthalpies of reaction for the production of OCSe and S and for the production
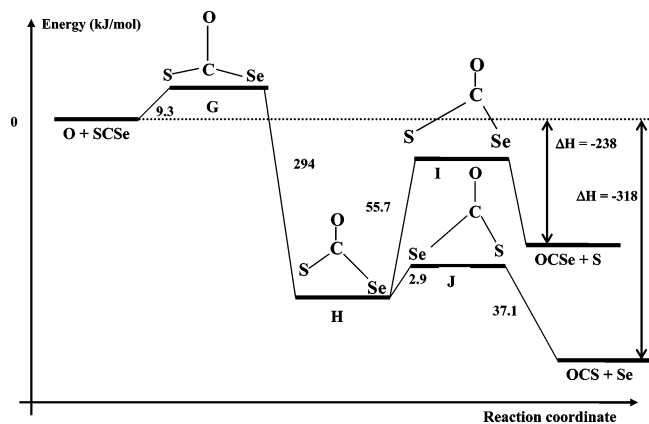
11822 *J. Phys. Chem. A, Vol. 109, No. 51, 2005*

Li et al.

Figure 8. Energy level diagram for the $O(^3P)$ + SCSe → OCS + Se(^3P) and OCSe + S(^3P) potential energy surfaces showing the intermediate and transition states computed at the UB3LYP/aug-cc-PVTZ level of theory.

of OCS and Se have been determined to be −238 and −318 kJ/mol, respectively. Interestingly, these values are very close to the corresponding values for the O/CS$_2$ and O/CSe$_2$ systems, indicating that the strength of a particular C=S or C=Se bond is almost the same in any of the carbon chalcogenides. The calculated activation barrier leading to its first transition state G is 9.3 kJ/mol, which is between the values for the O/CS$_2$ and O/CSe$_2$ systems. This again agrees with the experimental data in which decay of SCSe to OCS and OCSe is intermediate in rate compared to CS$_2$ and CSe$_2$. The transition state shows the O atom being located at almost right angle to the SCSe moiety. The intermediate COSeS denoted by H also possesses a relatively deep potential well, although this time it is no longer the lowest energy state of the reaction pathway. Further along the pathway, we managed to locate two more transition states, I and J which correspond to either the cleavage of the C−S bond to produce OCSe or the cleavage of the C−Se bond to produce OCS. As expected, the latter transition state, J is energetically lower by 53 kJ/mol since cleavage of the weaker C=Se bond is easier to achieve. However both transition states I and J are still lower in energy compared to G and may not play a critical role in determining the OCS/OCSe branching ratios. Experimental observations showed that the appearance rate of OCS is only slightly higher than the corresponding rate for OCS.

Rochford et al. has indicated from the transition-state structure that an angular attack of the O atom on OCS has taken place with an activation barrier of 24 kJ/mol for the production of CO and SO.[6] We have also assumed similar reaction pathways for the reaction of O with OCSe. Unfortunately an optimized transition-state structure could not be found despite a few attempts. Nevertheless, it is not surprising to expect the barrier to be lower than the O/OCS case by virtue of the weaker C=Se bond. Hence the reaction of O with OCSe should proceed much faster and in fact account for CO production in the system. However, CO$_2$ and Se may also be generated from the reaction of O with OCSe with a large release of energy (ΔH_r = 375 kJ/mol, also computed using UB3LYP/aug-cc-PVTZ). By virtue of its exothermicity, this channel could be deemed important although CO$_2$ could not be observed in the experiment. Hence, the same UB3LYP/aug-cc-PVTZ computations were carried out to trace its reaction pathway, and indeed, the transition state K was found to be located at about 85 kJ/mol higher than the reactants O and OCSe. The large value for the activation barrier appears to have hindered the formation of CO$_2$ under our experimental conditions.

Summary

We have determined the rate coefficients of the reactions of the carbon chalcogenides, CSe$_2$, SCSe, and OCSe with O(^3P) atom to be k_{CSe_2} = (1.4 ± 0.2) × 10^{-10} cm^3 molecule^{-1} s^{-1}, k_{SCSe} = (2.8 ± 0.3) × 10^{-11} cm^3 molecule^{-1} s^{-1}, and k_{OCSe} = (2.4 ± 0.3) × 10^{-11} cm^3 molecule^{-1} s^{-1} at 301−303 K using the technique of Fourier transform infrared (FTIR) absorption spectroscopy. These measurements have been carried out by using the known value of the rate coefficient for O(^3P) with CS$_2$ (4 × 10^{-12} cm^3 molecule^{-1} s^{-1}) as the internal calibrant. A main product channel yielding OCSe has been found for the O + CSe$_2$ reaction, similar to the O/CS$_2$ system. CO was also observed in the O/CSe$_2$ system, although its generation could be attributed to subsequent reactions of OCSe with O atoms. The corresponding reaction for O + SCSe gives roughly equal amounts of OCS and OCSe as products, although the dominant channel is still inferred to be the one that produces CSe and SO, and CS and SeO. Ab initio studies using density functional methods such as UB3LYP/aug-cc-PVTZ have been used particularly to determine the reaction pathways for the channels in which OCS or OCSe is produced.

References and Notes

(1) Tyndall, G. S.; Ravishankara, A. R. *Int. J. Chem. Kinet.* **1991**, *23*, 483.

(2) Cooper, W. F.; Hershberger, J. F. *J. Phys. Chem.* **1992**, *96*, 5405.

(3) Cheng, Y.; Han, J.; Chen, X.; Ishikawa, Y.; Weiner, B. R. *J. Phys. Chem. A* **2001**, *105*, 3693.

(4) Murakami, Y.; Kosugi, M.; Susa, K.; Kobayashi, T.; Fujii, N. *Bull. Chem. Soc. Jpn.* **2001**, *74*, 1233.

(5) Wei, C. N.; Timmons, R. B. *J. Chem. Phys.* **1975**, *62*, 3240.

(6) Rochford, J. J.; Powell, L. J.; Grice, R. *J. Phys. Chem.* **1995**, *99*, 15369.

(7) Naik, P. D.; Pavanaja, U. B.; Sapre, A. V.; Ramarao, K. V. S.; Mittal, J. P. *Chem. Phys. Lett.* **1991**, *186*, 565.

(8) Smith, I. W. M. *Discuss. Faraday Soc.* **1967**, *43−44*, 194.

(9) Morley, C.; Ridley, B. A.; Smith, I. W. M. *J. Chem. Soc., Faraday Trans. 2* **1972**, *68*, 2127.

(10) Pan, W. H.; Fackler, J. P., Jr. *Inorg. Synth.* **1982**, *21*, 6.

(11) Henriksen, L. *Synthesis* **1985**, *2*, 204.

(12) NIST Standard Reference Database No. 69, March, 2003. Release at: http://webbook.nist.gov/chemistry.

(13) Callear, A. B.; Tyerman, W. J. R. *Trans. Faraday Soc.* **1965**, *61*, 2395.

(14) *Molecular Spectroscopy: Modern Research*; Rao, K. N., Mathews, C. W., Eds.; Academic Press: New York, 1972−1985; Vol. 2, p 179.

(15) Frisch, M. J.; Trucks, G. W.; Schlegel, H. B.; Scuseria, G. E.; Robb, M. A.; Cheeseman, J. R.; Zakrzewski, V. G.; Montgomery, J. A., Jr.; Stratmann, R. E.; Burant, J. C.; Dapprich, S.; Millam, J. M.; Daniels, A. D.; Kudin, K. N.; Strain, M. C.; Farkas, O.; Tomasi, J.; Barone, V.; Cossi, M.; Cammi, R.; Mennucci, B.; Pomelli, C.; Adamo, C.; Clifford, S.; Ochterski, J.; Petersson, G. A.; Ayala, P. Y.; Cui, Q.; Morokuma, K.; Malick, D. K.; Rabuck, A. D.; Raghavachari, K.; Foresman, J. B.; Cioslowski, J.; Ortiz, J. V.; Baboul, A. G.; Stefanov, B. B.; Liu, G.; Liashenko, A.; Piskorz, P.; Komaromi, I.; Gomperts, R.; Martin, R. L.; Fox, D. J.; Keith, T.; Al-Laham, M. A.; Peng, C. Y.; Nanayakkara, A.; Gonzalez, C.; Challacombe, M.; Gill, P. M. W.; Johnson, B.; Chen, W.; Wong, M. W.; Andres, J. L.; Gonzalez, C.; Head-Gordon, M.; Replogle, E. S.; Pople, J. A. *GAUSSIAN 98*; Gaussian Inc.: Pittsburgh, PA, 1998.

(16) Hsu, D. S. Y.; Shaub, W. M.; Burks, T. L.; Lin, M. C. *Chem. Phys.* **1974**, *44*, 143.